Journal of Proteomics 140 (2016) 1–12

Contents lists available at ScienceDirect

Journal of Proteomics

journal homepage: www.elsevier.com/locate/jprot

Effects of Fe deficiency on the protein profiles and lignin composition of stem tissues from *Medicago truncatula* in absence or presence of calcium carbonate

Jorge Rodríguez-Celma [a,1], Giuseppe Lattanzio [a], Dido Villarroya [a], Elain Gutierrez-Carbonell [a], Laura Ceballos-Laita [a], Jorge Rencoret [b], Ana Gutiérrez [b], José C. del Río [b], Michael A. Grusak [c], Anunciación Abadía [a], Javier Abadía [a], Ana-Flor López-Millán [c,*]

[a] Plant Nutrition Department, Aula Dei Experimental Station (CSIC), P.O. Box 13034, E-50080, Zaragoza, Spain
[b] Instituto de Recursos Naturales y Agrobiología de Sevilla (CSIC), Reina Mercedes 10, E-41012 Sevilla, Spain
[c] USDA-ARS Children's Nutrition Research Center, Department of Pediatrics, Baylor College of Medicine, 1100 Bates Street, Houston, TX 77030, USA

ARTICLE INFO

Article history:
Received 14 December 2015
Received in revised form 7 March 2016
Accepted 10 March 2016
Available online 30 March 2016

Keywords:
Iron
Lignin
Microscopy
Stem
Petiole
Proteomics
Two-dimensional gel electrophoresis

ABSTRACT

Iron deficiency is a yield-limiting factor with major implications for crop production, especially in soils with high $CaCO_3$. Because stems are essential for the delivery of nutrients to the shoots, the aim of this work was to study the effects of Fe deficiency on the stem proteome of *Medicago truncatula*. Two-dimensional electrophoresis separation of stem protein extracts resolved 276 consistent spots in the whole experiment. Iron deficiency in absence or presence of $CaCO_3$ caused significant changes in relative abundance in 10 and 31 spots, respectively, and 80% of them were identified by mass spectrometry. Overall results indicate that Fe deficiency by itself has a mild effect on the stem proteome, whereas Fe deficiency in the presence of $CaCO_3$ has a stronger impact and causes changes in a larger number of proteins, including increases in stress and protein metabolism related proteins not observed in the absence of $CaCO_3$. Both treatments resulted in increases in cell wall related proteins, which were more intense in the presence of $CaCO_3$. The increases induced by Fe-deficiency in the lignin per protein ratio and changes in the lignin monomer composition, assessed by pyrolysis-gas chromatography–mass spectrometry and microscopy, respectively, further support the existence of cell wall alterations.

Biological significance: In spite of being essential for the delivery of nutrients to the shoots, our knowledge of stem responses to nutrient deficiencies is very limited. The present work applies 2-DE techniques to unravel the response of this understudied tissue to Fe deficiency. Proteomics data, complemented with mineral, lignin and microscopy analyses, indicate that stems respond to Fe deficiency by increasing stress and defense related proteins, probably in response of mineral and osmotic unbalances, and eliciting significant changes in cell wall composition. The changes observed are likely to ultimately affect solute transport and distribution to the leaves.

1. Introduction

Many environmental conditions, including the high pH of calcareous soils, can result in scarce Fe availability in farmlands, resulting in Fe-deficiency chlorosis and marked reductions in agricultural produce yield and quality [1–3]. Iron deficiency associated with soils rich in $CaCO_3$ is a major constraint for yield in economically relevant crops such as soybean grown in the upper Midwest areas of the U.S. [4–6] and fruit tree crops in Mediterranean climate areas [7,8]. When facing low soil Fe availability, plants respond by inducing root morphological and physiological changes aimed to increase the Fe uptake capacity, which vary depending on the taxonomical group [9]. Efforts have been devoted to deciphering this complex network in plants at the transcriptomic, proteomic and metabolomic levels [10–16]. In dicotyledonous plants, root responses include an induction of the Fe-reduction based uptake machinery [17,18], an enhanced proton extrusion capacity [19], the excretion of organic compounds including carboxylates, phenolics and flavins [15,20–23], and a reprogramming of general metabolic pathways such as the tricarboxylic acid cycle (TCA) and glycolysis to fuel the high energy requirements for Fe uptake [24,25]. Being an essential micronutrient, Fe must be translocated to the shoots, where it plays important roles in respiration and chlorophyll synthesis among others [26]. In the xylem pathway, complexation with citrate plays a determinant role [27–29].

The effects of Fe deficiency are not restricted to roots and leaves, and low soil Fe availability also results in plants with reduced stem length and mass [30]. Plant stems provide mechanical support to the plant and are essential for the delivery of water and nutrients (e.g., minerals, sugars

* Corresponding author.
E-mail address: lopezmil@bcm.edu (A.-F. López-Millán).
[1] Current address: John Innes Centre and University of East Anglia, Colney Lane, Norwich, NR4 7UH, U.K.

http://dx.doi.org/10.1016/j.jprot.2016.03.017
1874-3919/

and amino acids) to the various plant organs [31]. In addition, the vascular systems within the stem act as long distance communication channels between roots and shoots, in which hormones, micro-RNAs, peptides and proteins act as signaling molecules [32]. The dual role of these systems, including delivery of nutrients as well as signaling, makes stems crucial for the coordination of responses to nutritional stresses at the whole plant level. However, very little information is available to date about the effects of Fe deficiency in stem tissues.

Proteomic profiling using 2-DE is an excellent tool to provide a holistic picture of changes induced by nutritional stresses [32–34]. Indeed, changes in the protein profiles in response to Fe deficiency have already been studied in different plant tissues, mainly roots and thylakoids, using model plant species such as barrel medic (*Medicago truncatula*) [12]. This plant species has a small diploid genome that yields manageable genetic tools, it is autogamous, has a short generation time and a prolific seed production that makes it useful as a model legume [35–37]. Among the resources for *M. trucatula*, several reference proteomes, including that of stems, are currently available [37].

In the present study, we have examined the effects of Fe deficiency on the stem protein profiles of *M. truncatula* plants submitted to Fe deficiency, and used pyrolysis-gas chromatography–mass spectrometry and microscopy to assess changes in the lignin composition of these tissues. Legumes are valuable agricultural and commercial crops that serve as important nutrient sources for both humans and animals, and a better understanding of the effects of Fe deficiency in stems, essential for the long distance transport of Fe, may strengthen our ability to enhance Fe-efficiency responses. Two different treatments have been used to impose Fe deficiency in nutrient solution, with or without $CaCO_3$, with the aim to know whether the presence of $CaCO_3$, which is often found in Fe deficient soils, causes additional effects to those of a direct Fe shortage alone.

2. Material and methods

2.1. Plant material and growth conditions

Medicago truncatula cv. 'Jemalong' plants were grown in a controlled environment chamber with a photosynthetic photon flux density at leaf height of 350 μmol m^{-2} s^{-2} photosynthetically active radiation, 80% relative humidity and at a 16 h-23 °C/8 h-19 °C, day/night regime. Seeds were scarified by nicking the seed coat, then imbibed overnight in distilled water and germinated on filter paper for three days in darkness with full humidity. Seedlings were grown for an additional two-week period in half-strength Hoagland nutrient solution (pH 5.5) with 45 μM Fe(III)-EDTA [38]. Plants were then transplanted to 10 L plastic buckets (six plants per bucket) containing half-strength Hoagland nutrient solution and treatments were imposed. Control plants were grown with 45 μM Fe(III)-EDTA (pH 5.5) and Fe deficient plants were grown with no added Fe (0 μM Fe), with (pH 7.7) or without (pH 5.5) 1 g L^{-1} $CaCO_3$. After six days, stem tissues (including main stems and petioles but excluding cotyledons and leaves; Supplementary Fig. S1) were harvested, frozen in liquid N_2 and stored at −80 °C. Five independent batches of plants were grown and sampled for proteomic analysis. Tissues for mineral (stems including petioles, roots and leaves) and lignin (stems and petioles separately) analyses were also harvested six days after treatment onset from three plants per treatment in two independent batches of plants.

2.2. Protein extraction

For protein extraction, approximately 0.5–1 g of tissue (pooled from two plants of a given treatment), containing whole stems (including the main stems and petioles, see Supplementary Fig. S1) but excluding cotyledons and leaves, was ground in liquid N_2 with mortar and pestle. The tissue was homogenized in 6 mL of phenol saturated with 0.1 M Tris-HCl (pH 8.0) and containing 5 mM β-mercaptoethanol, by stirring for 30 min at 4 °C. Then, the homogenate was filtered (PVDF, 0.45 μm) and centrifuged at 5000 ×*g* for 15 min. The phenol phase was re-extracted for 30 min with one volume of phenol-saturated 0.1 M Tris-HCl (pH 8.0) containing 5 mM β-mercaptoethanol, and centrifuged as described above. Proteins in the phenol phase were precipitated by adding four volumes of 0.1 M ammonium acetate in cold methanol, followed by overnight incubation at −20 °C. Samples were then centrifuged at 5000 ×*g* for 15 min, and the pellet was washed three times with cold methanol, dried with N_2 gas and resuspended in sample rehydration buffer containing 8 M urea, 2% (w/v) CHAPS, 50 mM DTT, 2 mM PMSF and 0.2% (v/v) 3–10 ampholytes (Amersham, Uppsala, Sweden). After rehydration, samples were incubated at 38 °C for 1.5 h and then centrifuged at 15,000 ×*g* for 10 min at 20 °C. Samples were analyzed immediately by 2-DE. Protein concentration was measured with the Bradford method (BioRad kit), using microtiter plates in an Asys UVM 340 (Biochrom Ltd., Cambridge, U.K.) spectrophotometer and BSA as standard.

2.3. Protein 2-DE separation

Preliminary 2-DE experiments were carried out using a first dimension IEF separation with a linear pH gradient 3–10; in these conditions most of the spots were concentrated in the central region of the 2-DE gel (results not shown); therefore, to prevent protein co-migration and improve resolution a narrower pH gradient was chosen. A first dimension IEF separation was carried out on 7 cm ReadyStrip IPG Strips (BioRad) with a linear pH gradient pH 5–8 using a Protean IEF Cell (BioRad, Hercules, CA, USA). Strips were passively rehydrated for 16 h at 20 °C in 125 μL of rehydration buffer containing 60 μg of root extract proteins and a trace of bromophenol blue, and then transferred onto a strip tray. IEF was run at 20 °C, for a total of 14,000 V h (20 min with a 0–250 V linear gradient, 2 h with a 250–4000 V linear gradient and 4000 V until 10,000 V h). After IEF, strips were equilibrated for 10 min in equilibration solution I [6 M urea, 0.375 M Tris-HCl, pH 8.8, 2% (w/v) SDS, 20% (v/v) glycerol, 2% (w/v) DTT] and for another 10 min in equilibration solution II [6 M urea, 0.375 M Tris-HCl pH 8.8, 2% (*w/v*) SDS, 20% (v/v) glycerol and, 2.5% (w/v) iodoacetamide]. For the second dimension SDS-PAGE, equilibrated IPG strips were placed on top of vertical 12% SDS-polyacrylamide gels (8 × 10 × 0.1 cm) and sealed with melted 0.5% agarose in 50 mM Tris HCl, pH 6.8, containing 0.1% SDS. SDS-PAGE was carried out at 20 mA per gel for approximately 1.5 h, until the bromophenol blue reached the plate bottom, in a buffer containing 25 mM Tris, 192 mM glycine, and 0.1% SDS, at 4 °C. Gels were subsequently stained with colloidal Coomassie-blue G-250 (Serva, Barcelona, Spain). For each treatment, gels were made from independent whole stem samples (including petioles) preparations obtained from five different batches of plants ($n = 5$).

2.4. Gel image and statistical analysis

Stained gels were scanned with an Epson Perfection 4990 Photo Scanner (Epson Ibérica, Barcelona, Spain) at 600 dpi, previously calibrated using the SilverFast 6 software (LaserSoft Imaging AG, Kiel, Germany) and an IT8 reference card. Spot detection, gel matching and interclass analysis were performed with PDQuest 8.0 software (BioRad). First, normalized spot volumes based on total intensity of valid spots were calculated for each 2-DE gel and used for statistical calculations of protein abundance; for all spots present in the gels, pI, Mr, and normalized volumes (mean values and SD) were determined. Experimental MR values were calculated by mobility comparisons with Precision Plus protein standard markers (BioRad) run in a separate lane on the SDS gel, and pI was determined by using a linear scale over the total dimension of the IPG strips. Only spots consistently present in at least 80% of the replicates (four out of five gels) from at least one class were considered and used in further analysis; missing spot volumes were estimated from the data set by a sequential K-Nearest

Neighbor algorithm using an R 2.7.0 environment. After the input of missing values, a second normalization based on total intensity of valid spots per gel was used to compensate for gel replicate variations, and resulting data were used for statistical analyses. The spots were also manually checked, and consistent reproducibility between normalized spot volumes was found in the different replicates (Supplementary Table S1).

Univariate and multivariate statistical analyses were carried out. Spots changing in relative abundance were selected using a paired Student *t*-test and a significance level of $p < 0.05$. Protein response ratios were defined as the relative abundance in a given treatment divided by the relative abundance in the controls. Only proteins with mean response ratios above 2.0 or below 0.5 were considered as physiologically relevant and are discussed in this study. Principal component analysis (PCA) was carried out using Excel ad-in Multibase 2014.

2.5. Protein identification by nano-liquid chromatography-tandem mass spectrometry (nLC-ESI-MS/MS)

Consistent spots showing statistically significant differences in accumulation were excised automatically using a spot cutter EXQuest (BioRad), proteins in spots digested, and peptides separated by nano-HPLC (n-HPLC system 1200 series, Agilent Technologies, Waldbronn, Germany) as described in [39]. The nano-HPLC was connected to a HCT Ultra high-capacity ion trap (Bruker Daltonics, Bremen, Germany) using a PicoTip emitter (50 μm i.d., 8 μm tip i.d., New Objective, Woburn, MA, USA) and an online nano-electrospray source. Capillary voltage was −1.8 kV in positive mode and a dry gas flow rate of 10 L min^{-1} was used with a temperature of 180 °C. MS data were acquired automatically using Hystar 3.2 software following a MS survey scan from 50 to 3000 *m/z* at a resolution of 5500. The mass window for precursor ion selection was ±0.15 m/z with an active exclusion after two spectra and release after 1.2 min for the one most intense peptide. MS/MS spectra were sequentially and dynamically acquired in a scan from 300 to 1500 m/z with a maximum accumulation time of 750 ms depending on sample concentration. The fragmentation amplitude for MS/MS was 1 V. Singly charged ions and trypsin peptides were excluded from MS/MS analysis. Peak detection, deconvolution and processing were performed with Data Analysis 3.4 (Bruker Daltonics).

Protein identification was carried out using the Mascot search engine (version 2.3.02, Matrix Science; London, UK) and the non-redundant databases NCBInr 20,120,303 (17,378,729 sequences; 5,967,463,365 residues). Search parameters were: monoisotopic mass accuracy, peptide mass tolerance ±0.2 Da, fragment mass tolerance ±0.6 Da; one allowed missed cleavage; allowed fixed modification carbamidomethylation (Cys), and variable modification oxidation (Met). Positive identification was assigned with Mascot scores above the threshold level ($p \leq 0.05$) and at least two identified peptides with a score above homology. The list of peptides identified is shown in Supplementary Table S2. We used the GO biological process annotation (http://www.geneontology.org) of the individual identified proteins and UniProt database information for manual classification into functional categories.

2.6. Mineral analysis

Roots, whole stems (including petioles) and leaves were harvested from three plants per treatment, dried in a conventional oven at 60 °C and ground in a stainless steel mill. Subsamples (ca. 0.15 g dry weight) of each ground sample were digested and processed for elemental analysis as described elsewhere [40]. Elemental analysis (Ca, Cu, Fe, K, Mg, Mn, Mo, Na, P, S, and Zn) was carried out using inductively coupled plasma-optical emission spectroscopy (CIROS ICP Model FCE12; Spectro, Kleve, Germany); the instrument was calibrated daily with certified standards. Tomato leaf standards (SRM 1573 A; National Institute of Standards and Technology, Gaithersburg, MD, USA) were digested and analyzed along with the *M. truncatula* samples to ensure accuracy.

2.7. Microscopy

For microscopy analysis, sections from both petioles and stems of *M. truncatula* plants grown for 6 d in the control conditions or with 0 μM Fe in the presence or absence of $CaCO_3$, were excised with a razor blade and embedded in 5% agar. Eight different petiole and stem sections from eight different plants for each treatment were analyzed. Stem and petiole transversal sections (60 μM thick) were obtained using a vibrating blade microtome (VT1000 S, Leica Microsystems GmbH). Cell walls were stained using phloroglucinol (SIGMA), and bright field and auto-fluorescence images of the transversal slices were taken with an inverted microscope (DM IL LED, Leica Microsystems GmbH) equipped with a fluorescence kit (340–380 excitation wavelength and 425 nm cut-off filter; *A*1 filter cube, Leica Microsystems GmbH) and a CCD camera (DFC 240C, Leica Microsystems GmbH).

2.8. Lignin analysis

Lignin analysis was carried out by pyrolysis-gas chromatography–mass spectrometry (Py-GC–MS) using separately petioles and stems harvested from three *M. truncatula* plants per treatment. Pyrolysis of the samples (approximately 7 mg) was performed with a 3030 μ-furnace pyrolyzer (Frontier Laboratories Ltd.) connected to an Agilent 7820 A GC using a DB-1701 fused-silica capillary column (60 m × 0.25 mm i.d., 0.25 μm film thickness) and an Agilent 5975 mass selective detector (EI at 70 eV). The pyrolysis was performed at 500 °C. The oven temperature was programmed from 45 °C (4 min) to 280 °C (10 min) at 4 °C min^{-1}. Helium was the carrier gas (2 mL min^{-1}). Compounds were identified by comparing their mass spectra with those in the Wiley and NIST libraries and those reported in the literature [41]. Peak molar areas were calculated for the main lignin-degradation products using their characteristic mass fragment ions, the summed areas were normalized, and data from four biological replicates were averaged and expressed as percentages. The main lignin compounds and the mass fragment ions used for quantitation were: guaiacol (m/z 124), 4-methylguaiacol (m/z 138), 4-ethylguaiacol (m/z 137), 4-vinylguaiacol (m/z 150), eugenol (m/z 164), *cis*-isoeugenol (m/z 164) and *trans*-isoeugenol (m/z 164) as guaiacyl-lignin markers, and syringol (m/z 154), 4-methylsyringol (m/z 168), 4-ethylsyringol (m/z 167), 4-vinylsyringol (m/z 180), 4-allylsyringol (m/z 194), *cis*-4-propenylsyringol (m/z 194), and *trans*-4-propenylsyringol (m/z 194) as syringyl-lignin markers. The compounds used for quantitation of proteins and their characteristic fragment ions were phenylacetonitrile (m/z 117), indole (m/z 117), and 3-methylindole (m/z 130).

3. Results

Symptoms of Fe deficiency in *M. truncatula* plants included a yellowing of young leaves and a reduction of biomass, which were more intense in the treatment that included $CaCO_3$; these symptoms were described in detail in a parallel study focused to root proteomic changes [42].

3.1. Protein profiles

Changes in the protein profile of extracts of stems (including petioles) from Fe deficient *M. truncatula* plants grown in the absence (pH 5.5) or presence of $CaCO_3$ (pH 7.7) were studied by 2-D IEF-SDS PAGE electrophoresis. Typical real scans of 2-DE gels obtained from root protein extracts of Fe-sufficient and Fe-deficient (pH 5.5 or 7.7) plants are shown in Fig. 1A-C, respectively. The average number of detected spots (mean ± SD) was 265 ± 2, 261 ± 2 and 267 ± 2 in gels

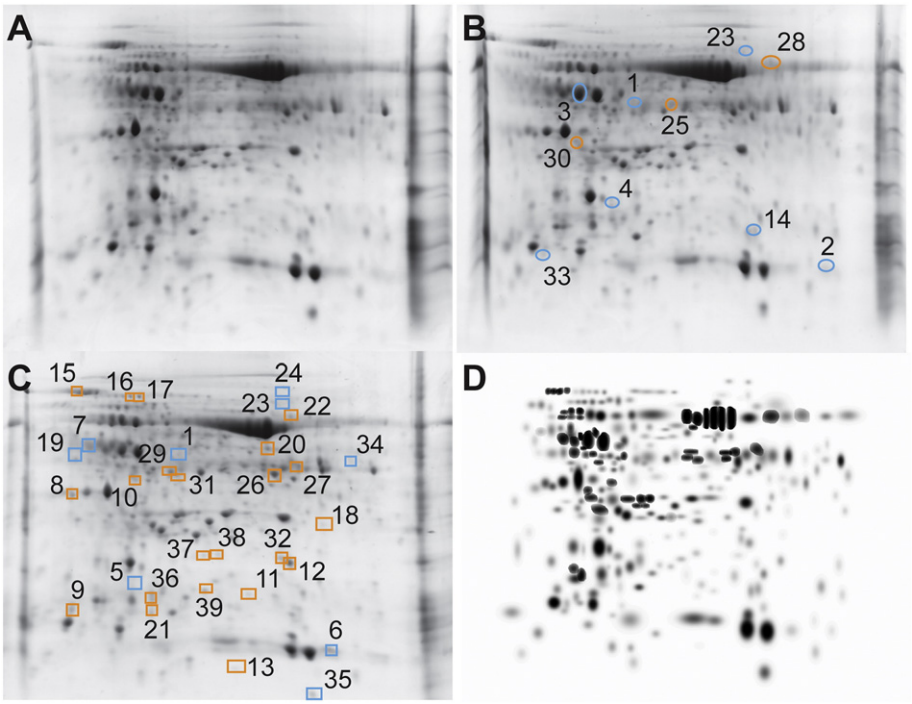

Fig. 1. 2-DE IEF-SDS PAGE protein profile maps of stem extracts from *Medicago truncatula* plants. Scans of typical gels from the stems of Fe-sufficient and Fe-deficient plants grown in the absence and presence of $CaCO_3$ are shown in A, B and C, respectively. To facilitate visualization of the studied spots, a virtual composite image (D) was created containing all spots present in the real gels A, B and C. In B (−Fe) and C (−Fe + $CaCO_3$), spots whose intensities decreased or increased when compared to control maps are marked with blue and orange symbols, respectively. Identified spots are labeled in B and C with the corresponding number assigned in Table 1.

from plants grown with 45 μM Fe and 0 μM Fe in the absence or presence of $CaCO_3$; approximately 95% of spots were consistently found in all five replicates within each treatment (Supplementary Table S3). The total number of spots consistently detected in the whole experiment (present in at least 80% of the gels of one treatment) was 276 (Supplementary Tables S1 and S3). A composite averaged virtual map containing all spots present in all 15 gels (5 per treatment) is shown in Fig. 1D.

When compared to the control plants, four and 11% of the consistent spots (10 and 31 spots, respectively) showed changes in relative abundances that were statistically significant at $p < 0.05$ and above the cut-off values for fold-change (≥2 or ≤0.5) in the 0 μM Fe treatments in the absence or presence of $CaCO_3$, respectively (these spots are marked in bold and with an asterisk in Table 1). Two of these changes (decreases in the relative abundance of spots *1* and *23*) occurred irrespectively of the presence of $CaCO_3$ (Table 1 and Fig. 2B). From the total 39 spots showing physiologically relevant changes, 80% (31 spots) were reliably identified (Table 1). When a PCA analysis was run using all consistent spots, the samples from Fe-deficient plants in the presence of $CaCO_3$ were well separated, whereas those from Fe sufficient plants and Fe-deficient plants grown without $CaCO_3$ overlapped (Fig. S2A). However, when the PCA analysis was run using only those spots showing significant differences in relative abundance, samples from the three treatments were clearly separated (Fig. S2B).

The statistical analysis of averaged maps indicated that the Fe deficiency treatment in absence of $CaCO_3$ caused significant increases ($p < 0.05$; fold-change ≥2) in relative abundance of three spots (spots *25*, *28* and *30* in Table 1; orange ellipses in Fig. 1B). All of them matched reliably to known proteins and were manually classified by their GO: BP (Biological Process) annotation to general metabolism (spots *25* and *28*) and phenylpropanoid metabolism (spot *30*) (Fig. 2A). Five spots (spots *1–3*, *14* and *23*) showed significant decreases in relative abundance and two more (spots *4* and *33*) were no longer detected in the 0 μM Fe treatment when compared to controls ($p < 0.05$; fold-change ≤0.5; blue ellipses in Fig. 1B), and six of them were reliably identified (spots labeled *1–4*, *14* and *23* in Table 1); they were assigned to photosynthesis (spots *1–4*), protein modification (spot *14*) and oxidation/reduction process (spot *23*) (Fig. 2A).

Changes in the whole stem protein profile were more marked when Fe deficiency was imposed in the presence of $CaCO_3$. Eighteen spots showed significant increases in relative abundance (spots *8–12*, *15–18*, *20*, *21*, *26*, *27*, *32*, and *36–39* in Table 1) and four more were detected *de novo* (spots *13*, *22*, *29* and *31* in Table 1) in the Fe deficient treatment in the presence of $CaCO_3$ when compared with the controls ($p < 0.05$; fold-change ≥2; orange rectangles in Fig. 1C). Among them, 17 were reliably identified and manually classified in the following functional categories: photosynthesis (spot *8*), defense and oxidative stress (spots *9–13*), protein metabolism (spots *15–18*, *20* and *21*), oxidation/reduction processes (spot *22*), general metabolism (spots *26* and *27*) and secondary metabolism (spots *29* and *31*) (Table 1, Fig. 2A). Six spots showed significant decreases in relative abundance (spots *1*, *6*, *7*, *23*, *24* and *35* in Table 1) and three more (spots *5*, *19* and *34* in Table 1) were no longer detected ($p < 0.05$; fold-change ≤0.5; blue rectangles in Fig. 1C). Among them, seven spots were identified and assigned to photosynthesis (spots *1* and 5–*7*), translation (spot *19*), and oxidation-reduction process (spots *23* and *24*) (Fig. 2A).

The information on the significant changes ($p < 0.05$; fold-change ≥2 or ≤0.5) in protein abundance as a result of both Fe deficiency treatments is summarized in a Venn diagram (Fig. 2B), using the same color code than that used in Fig. 1 (orange and blue numbers for increases and increases in relative abundance, respectively). Two spots (spots *1* and *23* in Table 1) changed significantly and above the cut-off values in both Fe-deficiency treatments.

3.2. Mineral analysis

Mineral analysis was carried out in whole stem samples (including stems and petioles). The stem dry weights from Fe-deficient plants

Table 1
Proteins identified in 2-D IEF-SDS PAGE gels. In the −Fe vs +Fe and −Fe + $CaCO_3$ vs +Fe columns, spots showing statistically significant changes (*t*-Student's test, $p < 0.05$) and above the biological relevant cut-off values (fold ≥2 or fold ≤0.5) are marked in bold with an asterisk, and spots showing significant changes in relative abundance but with fold-changes outside the cut-off values are marked only in bold. For some spots, fold changes outside the threshold cut off values ($p < 0.05$ and/or fold ≥2 or fold ≤0.5) are indicated in normal typeface in a given treatment when they were significant in the other treatment. Spots were analyzed by LC-MS/MS and positive identification was retained with Mascot scores (Sc) above the threshold levels ($p < 0.05$) and at least two identified peptides with a ion score above homology (ion/pep). Function was inferred from GO and UniProt entry annotation. "new" and "lost" indicate spots that have been newly detected or no longer detected in the −Fe treatments.

Spot n	UniProt identifier	Protein description	Species	Mascot output (Sc/ion/pep)	Sq %	Theor Mw/pI	Exp Mw/pI	−Fe vs +Fe	−Fe + $CaCO_3$ vs +Fe	GO:BP
Photosynthesis										
1	Q40073	Rubisco activase A	*Hordeum vulgare*	162/2/2	8	47/8.6	44/6.2	**0.2***	**0.1***	Photosynthesis (GO:0015979)/ ATP binding (GO:0005524)
2	B7FMC2	Rubisco small chain 3A	*M. truncatula*	343/10/6	44	20/8.7	16/7.3	**0.2***	**0.7**	Photosynthesis (GO:0015979)/ C fixation (GO:0015977)
3	A0A072UZ59	Rubisco activase	*M. truncatula*	975/53/15	45	48.0/6.9	43/5.7	**0.5***	**0.6**	Photosynthesis (GO:0015979)/ Reductive pentose-phosphate cycle (GO:0019253)
4	P28459	Rubisco large chain	*Viburnum acerifolium*	62/2/2	4	53/6.1	25/5.9	**lost***	0.7	Photosynthesis (GO:0015979)/ Reductive pentose-phosphate cycle (GO:0019253)
5	B7FGU7	Cytochrome b6-f complex iron-sulfur subunit	*M. truncatula*	156/2/2	11	24/7.6	23/5.9	0.3	**lost***	Photosynthetic electron transport chain (GO:0,009,767)
6	KEH21532	Rubisco small chain	*M. truncatula*	275/14/6	37	20.4/8.7	16/7.6	0.2	**0.2***	Photosynthesis (GO:0015979)/ C fixation (GO:0015977)
7	Q8GTY4	Rubisco activase	*M. sativa*	480/10/6	39	30/5.6	43/5.4	1.8	**0.5***	Photosynthesis (GO:0015979)/ ATP binding (GO:0005524)
8	P14226	Oxygen-evolving enhancer protein 1	*P. sativum*	141/3/3	13	35/6.25	30/5.2	**1.5**	**2.2***	Photosynthesis (GO:0015979)/ Photosystem II stabilization (GO:0042549)
Defense/response to oxidative stress										
9	B7FKA0	Polyketide cyclase/dehydrase and lipid transporter	*M. truncatula*	148/3/3	24	18/5.1	20/5.5	0.9	**2.1***	Defense response (GO:0006952)/ mRNA modification (GO:0016556)
10	A6XJ26	Thioredoxin reductase	*M. truncatula*	155/2/2	7	40/6.9	34/5.8	1.4	**2.8***	Removal of superoxide radicals (GO:0019430)
11	Q56VU1	Glutathione peroxidase 1	*L. japonicus*	125/3/2	9	26/8.8	22/6.7	2.9	**3.7***	Response to oxidative stress (GO:0006979)
12	B6ZHC0	PR-5b protein	*Glycine max*	159/3/2	17	27/6.3	27/7.0	2.8	**12.4***	Phatogenesis related
13	A0A072TXU3	Glutaredoxin C4	*M. truncatula*	108/2/2	34	11.4/6.5	14/6.6	new	**new***	Cell redox homeostasis (GO:0045454)
Protein-related process										
14	B7FF81	Ubiquitin-conjugating enzyme	*M. truncatula*	77/2/2	14	17/6.2	20/7.1	**0.4***	0.9	Protein ubiquitination (GO:0016567)
15	P49118	78 kDa glucose-regulated protein homolog	*Solanum lycopersicum*	367/5/4	13	41/8.5	74/5.4	**1.4**	**2.1***	Protein folding (GO:0006457)
16	G7JU14	Heat shock 70 kDa protein	*M. truncatula*	887/16/13	24	72/5.9	70/5.8	1.2	**2.3***	Protein folding (GO:0006457)
17	P37900	Heat shock 70 kDa protein. mitochondrial	*P. sativum*	241/6/4	8	72/5.8	70/5.8	1.2	**2.5***	Protein folding (GO:0006457)
18	P38548	GTP-binding nuclear protein Ran/TC4	*Vicia faba*	175/5/4	19	25.6/6.4	29/7.3	lost	**6.1***	Small GTPase mediated signal transduction (GO:0007264)/ Protein transport (GO:0015031)
19	XM_003594608	30S ribosomal protein S1	*M. truncatula*	297/5/5	18	44.9/5.2	44/5.3	1.0	**lost***	Translation (GO:0006412)
20	D7KCE2	Elongation factor Tu	*A. lyrata*	366/10/6	15	49/6.6	43/6.8	1.1	**2.8***	Translational elongation (GO:0006414)
21	G7LE33	40S ribosomal protein S12	*M. truncatula*	218/6/5	51	15.6/5.5	20/6.0	0	**22.9***	translation (GO:0006412)
Oxidation/reduction process										
22	O81413	Ferric leghemoglobin reductase-2	*G. max*	278/7/6	14	53/6.9	51/7.0	nd	**New***	Cell redox homeostasis (GO:0045454)
23	G7JL79	Ferredoxin-nitrite reductase	*M. truncatula*	223/4/4	9	65.8/6.5	64/7.0	**0.2***	**0.3***	Nitrate transport (GO:0015706)/ Cysteine biosynthetic process (GO:0019344)/ Oxidation-reduction process (GO:0055114)
24	G7J8R4	NADH-ubiquinone oxidoreductase 75 kDa subunit	*M. truncatula*	310/5/5	8	82/7.1	74/7.0	0.7	**0.4***	Respiratory chain complex I (GO:0045271)/ Proteasome core complex assembly (GO:0080129)/ Oxidation-reduction process (GO:0055114)/ ATP synthesis coupled electron transport (GO:0042773)/ Response to oxidative stress (GO:0006979)/ Gravitropism (GO:0009630)
Metabolism										
25	Q9FT00	Malate dehydrogenase 2	*C. arietinum*	71/2/2	8	36/5.9	43/6.4	**4.8***	2.5	Tricarboxylic acid cycle (GO:0006099)/ Carbohydrate metabolic process

(continued on next page)

Table 1 (*continued*)

Spot n	UniProt identifier	Protein description	Species	Mascot output (Sc/ion/pep)	Sq %	Theor Mw/pI	Exp Mw/pI	−Fe vs + Fe	−Fe + $CaCO_3$ vs + Fe	GO:BP
										(GO:0005975)
26	O48904	Malate dehydrogenase precursor	*M. sativa*	541/12/7	24	36/8.8	36/6.9	1.0	**2.6***	Tricarboxylic acid cycle (GO:0006099)/ Carbohydrate metabolic process (GO:0005975)
27	B7FJQ4	Malate dehydrogenase	*M. truncatula*	351/11/5	13	36/6.1	42/7.1	2.2	**2.7***	Tricarboxylic acid cycle (GO:0006099)/ Carbohydrate metabolic process (GO:0005975)
28	A9YWS0	Serine-hydroxymethyl-transferase	*M. truncatula*	87/2/2	7	58/8.4	52/7.2	**3.1***	**1.5**	Serine (GO:0006563) and glycine (GO:0006544) metabolic process / One C metabolism (GO:0006730)/ Methylation (GO:0032259)
Secondary metabolism										
29	B7FHV0	Phenylcoumaran benzylic ether reductase-like protein Fi1	*M. truncatula*	358/6/6	27	33.9/5.6	42/6.1	nd	**new***	Oxidation-reduction process (GO:0055114) / Phenylpropanoid metabolic process (GO:0009698)
30	B7FIC1	Putative *O*-methyltransferase	*M. truncatula*	114/4/4	23	28/5.4	30/5.7	**3.8***	4.6	Methylation (GO:0032259)/ Phenylpropanoid metabolic process (GO:0009698)/ Cysteine biosynthetic process (GO:0019344)
31	Q45FF2	pyridoxal biosynthesis protein PDX1.3	*M. truncatula*	334/8/4	16	34/5.6	35/6.2	nd	**new***	Pyridoxal phosphate biosynthetic process (GO:0042823)
Not identified										
32		Not identified					27/6.9	**1.4**	**2.3***	
33		Not identified					17/5.5	**lost***	1.1	
34		Not identified					43/7.5	0.4	**lost***	
35		Not identified					13/7.1	0.7	**0.4***	
36		Not identified					22/5.9	1.0	**2.0***	
37		Not identified					28/6.3	1.7	**2.3***	
38		Not identified					28/6.5	1.0	**2.4***	
39		Not identified					23/6.4	1.2	**3.2***	

grown in both conditions were approximately 24% lower than that of the Fe-sufficient controls (Fig. 3A). Iron concentration in stems of Fe-deficient plants grown in the absence of $CaCO_3$ did not change when compared to controls, whereas in Fe-deficient plants grown in the presence of $CaCO_3$ the Fe concentration was 54% lower than in Fe-sufficient controls (Fig. 3B). The total Fe content in stems was lower in both Fe deficiency treatments when compared to controls, due to the lower stem dry weights in the absence of Fe (Supplementary Fig. S3). Stem concentrations of Zn, Cu and Mn from Fe-deficient plants grown in the absence of $CaCO_3$ were 90, 100 and 60% higher, respectively, than those in the Fe-sufficient controls, whereas the concentrations of Ni, Mo, Co and B did not change significantly (Fig. 3B). The presence of $CaCO_3$ in the zero-Fe solution did not lead to significant changes in the concentrations of Zn, Cu, Mn, Ni, Mo Co and B when compared to the Fe-sufficient controls (Fig. 3B).

With regard to macronutrient concentrations, in whole stems of Fe deficient plants grown in the absence of $CaCO_3$ the only significant change was a 50% increase in Mg concentration when compared to Fe-sufficient controls (Fig. 3C). In the presence of $CaCO_3$, increases in Mg (140%), and Ca (28%) concentrations and a decrease in K concentration (10%) were found when compared to those in Fe sufficient controls (Fig. 3C).

The mineral composition of leaves and roots was also determined (Supplementary Fig. S4). In roots, Fe concentration was lower than in controls in both Fe deficiency treatments, whereas Zn and Cu concentrations increased in the absence of $CaCO_3$ and Ni concentration increased in the presence of $CaCO_3$. In leaves, Fe concentration only decreased in the presence of $CaCO_3$. Regarding other micronutrients in leaves, results were similar to those described above for stems, with Zn, Cu, Mn and also Ni concentrations being higher in the Fe-deficiency treatment in the absence of $CaCO_3$ than in Fe-sufficient controls, and similar to controls or only slightly higher in the presence of $CaCO_3$ (Supplementary Fig. S4). The trends observed for changes in macronutrient concentrations in leaves and roots as a result of both Fe deficiency treatments were quite similar to those observed in stems (Supplementary Fig. S4). The only significant changes in macronutrient root concentrations occurred in Fe-deficient plants in the presence of $CaCO_3$, and included an increase in Ca and decreases in P and S concentrations (Supplementary Fig. S4). In leaves, Fe deficiency increased Ca and Mg concentrations, with the increases being larger in the presence of $CaCO_3$.

3.3. Microscopy of petiole and stem sections

In order to study possible cell wall changes, lignin was localized in sections of stems and petioles using autofluorescence and phloroglucinol staining. In Fe-sufficient petioles, the blue autofluorescence signal was mainly detected in xylem vessels and sclerenchyma tissue (Fig. 4A). When compared to controls, Fe-deficient petioles from plants grown in the absence of $CaCO_3$ showed a slightly lower autofluorescence intensity in both xylem vessel and sclerenchyma tissue (Fig. 4B), whereas in petiole sections from Fe-deficient plants grown in the presence of $CaCO_3$, the autofluorescence signal intensity decreased in xylem vessels when compared to both sclerenchyma and controls (Fig. 4C). This decrease in autofluorescence occurred especially in the innermost part of xylem vessels, where blue autofluorescence was barely observed and instead a greenish color was detected (Fig. 4C).

When phloroglucinol staining was used, lignin distribution in Fe-sufficient petioles was similar to that found using autofluorescence, but the staining was more intense in the sclerenchyma (deep red) than in xylem vessels (almost black) (Fig. 4D). Phloroglucinol staining of Fe-deficient petioles from plants grown in the absence of $CaCO_3$ yielded an intense coloration in xylem vessels similar to that observed in Fe-sufficient controls and little staining in the sclerenchyma (Fig. 4E). In petiole sections from Fe-deficient plants grown in the presence of $CaCO_3$, phloroglucinol staining was intense and even higher

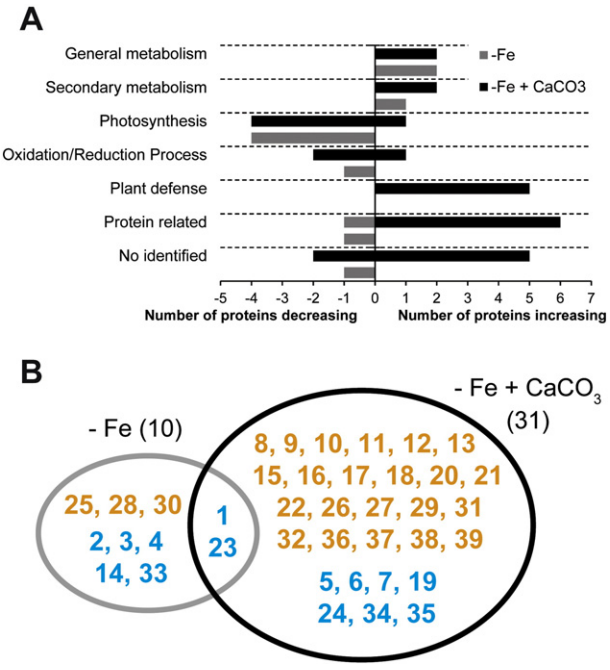

Fig. 2. A. Number of identified spots changing as a result of Fe deficiency, organized in metabolic pathways. Pathways related to the identified proteins were integrated according to the UniProt database and GO annotation. B. Venn diagram depicting proteins with changes in abundance as a result of the Fe deficiency treatments. Numbers indicate spots as in Table 1. Orange and blue color numbers indicate increases (including new appearances) and decreases (including disappearances) in spot abundance as a result of Fe deficiency, respectively.

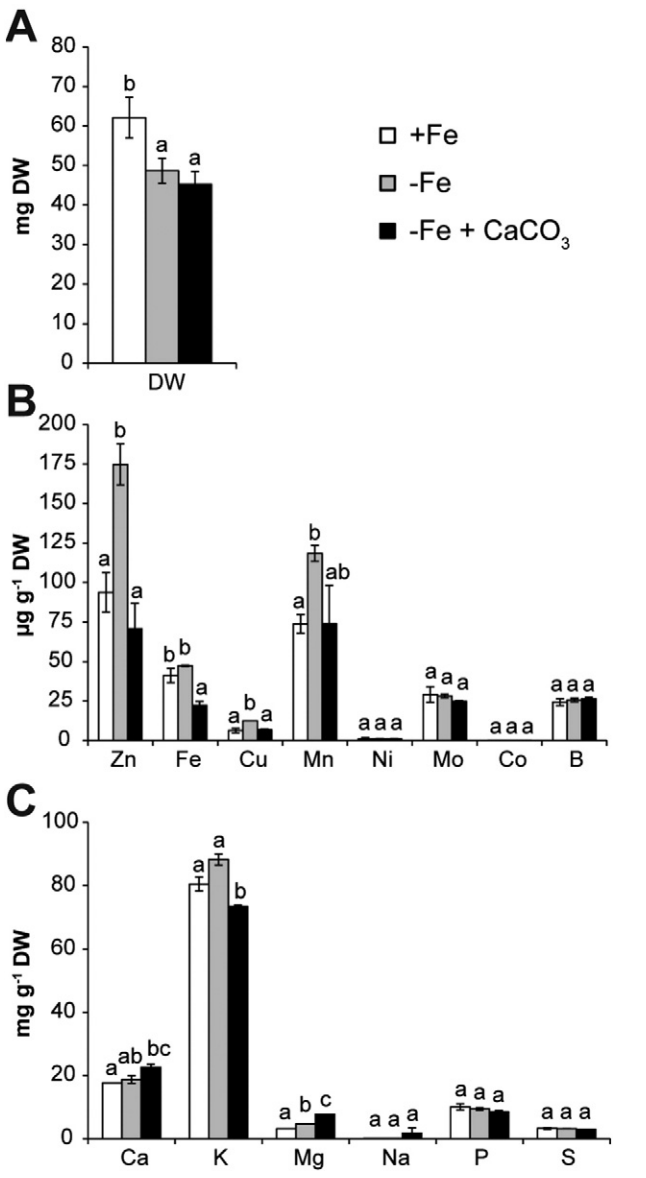

Fig. 3. Mineral composition of stems, including petioles, as affected by Fe deficiency. A: dry mass (DW, in mg per plant); B: micronutrient concentrations (in µg g^{-1} DW), and C: macronutrient concentrations (in mg g^{-1} DW) of stems (including petioles) of *Medicago truncatula* plants grown for six days in Fe-sufficient (white columns) and Fe-deficient conditions (grey columns for plants grown in the absence of $CaCO_3$ and black columns for plants grown in the presence of $CaCO_3$). Data are means ± SE ($n = 3$; from one batch of plants with three samples per treatment). Columns marked with the same letter are not significantly different at the $p \leq 0.05$ probability level.

than that observed in controls in both xylem vessels and sclerenchyma (Fig. 4F).

Stems of Fe-sufficient plants showed a clear blue autofluorescence in the xylem vessels and a more diffuse one in the cortex, and similar results were observed when phloroglucinol was used for lignin staining (Supplementary Fig. S5). Stems from Fe deficient plants showed similar autofluorescence and staining patterns to those of controls, irrespective of the presence of $CaCO_3$ in the nutrient solution (Supplementary Fig. S5).

3.4. Lignin analysis

The lignin composition (relative molar abundances of G- and *S*-lignin derived markers and S/G ratios) of both stems and petioles samples was studied by Py-GC/MS. The percentages of protein markers relative to the lignin markers (lignin/protein ratio) were also estimated.

In petioles, the lignin per protein ratio increased 20 and 110% in the Fe deficiency treatment in the absence and presence of $CaCO_3$, respectively, when compared to the Fe-sufficient controls (Table 2). The total relative abundance of S- and G- lignin markers and the S/G ratio in petioles from both Fe deficiency treatments were similar to those of controls but significantly different between them (Table 2). However, the relative molar abundances for most of the specific G lignin markers (six of the seven compounds measured) in Fe-deficient samples presented statistically significant differences (two compounds increased and four compounds decreased with Fe deficiency) with those of control samples (Table 2). The relative molar abundances of specific S-lignin markers changed in at least one of the Fe-deficiency treatments in four of the seven measured compounds when compared to control petioles (Table 2).

On the other hand, very few changes in the stem lignin parameters were found with Fe deficiency. The lignin per protein ratios, relative molar abundances of G- and S-lignin derived markers and S/G ratios were similar in the Fe-deficient samples, irrespective of the presence of $CaCO_3$, to those found in Fe-sufficient controls (Table 2).

4. Discussion

In the present study we have characterized the differences in the protein profiles of whole stems (including petioles) from *M. truncatula* plants grown in hydroponics in two different Fe deficiency conditions, in the presence and absence of $CaCO_3$, with the aim of shedding light into processes that may be relevant in Fe deficiency induced modifications in this tissue. It should be noted that the individual specific effects of Fe deficiency and $CaCO_3$ in the proteome of stems from Fe-deficient plants grown in the presence of $CaCO_3$ cannot be discriminated using the current experimental approach. The presence of $CaCO_3$ along with

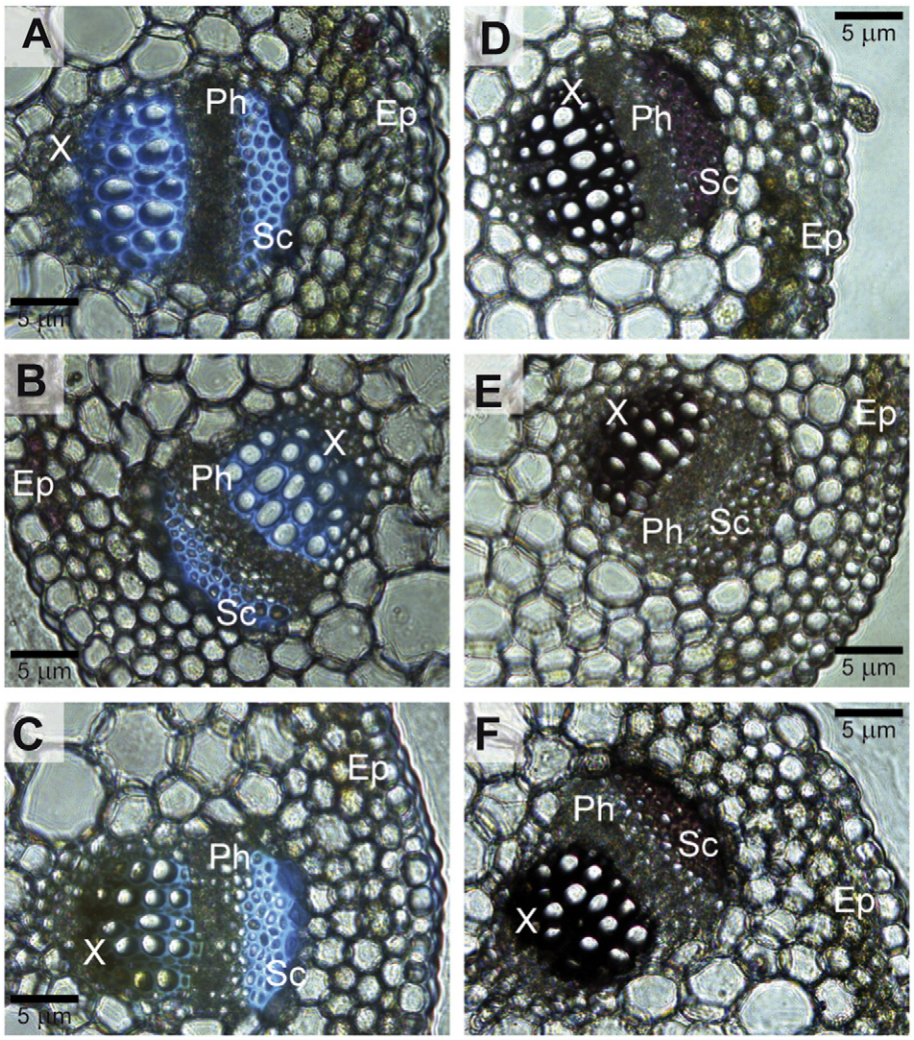

Fig. 4. Microscopy analyses of Fe-deficient petioles. Micrographs of petiole sections (10×): autofluorescence (A–C) and phloroglucinol staining (D–F) from Fe-sufficient plants (A and D) and Fe-deficient plants grown in the absence (B and E) and presence of $CaCO_3$ (C and F). X: xylem; Ph: phloem; C: cortex; Ep: epidermis, and Sc: sclerenchyma. Transversal petiole slices, 60 µm thick, were obtained using a vibrating blade microtome.

Fe(III)-EDTA as an Fe source causes Fe precipitation and immobilization, therefore making unfeasible its use as a control.

Overall results from the protein profiling indicate that Fe deficiency in the presence of $CaCO_3$ has a more pronounced impact on the stem proteome than the lack of Fe alone, since a larger number of spots (31) displayed differences in relative accumulation in the presence of $CaCO_3$ than in its absence (10). This stronger effect is also supported on one hand by the fact that the functional category containing the most spots that increased in relative abundance (five) in Fe-deficient plants grown in the presence of $CaCO_3$ was the defense and stress category, whereas in the absence of $CaCO_3$ no proteins from this category were found to increase significantly (Fig. 2A and Table 1). A similar situation was described in the proteomic profiling of roots of in the same plant species [42]; this is not only the result of the lack of Fe and the presence of $CaCO_3$, but also of a combination of factors including the basic pH of the growing solution which impairs Fe mobilization in the root apoplast [3,43,44]. Furthermore, the presence of $CaCO_3$ may alter the pH of plant fluids such as the xylem sap and apoplastic fluid causing changes in the chemical speciation of Fe and therefore in Fe availability [45,46,47]. On the other hand, the functional category containing most of the spots decreasing in relative abundance was photosynthesis, with six proteins decreasing in relative abundance in the presence of $CaCO_3$ (four of them above and two below the biological cut-off value) in comparison with the four decreasing in the absence of $CaCO_3$. The decreases in the relative abundance of the photosynthesis related proteins affect different isoforms of the Rubisco activase (spots *1*, *3* and *7*; Supplementary Fig. S6A), the large (spot *4*) and small chains (spots *2* and *6*) of Rubisco, and the iron-sulfur subunit of the cytochrome b6-f complex (spot *5*), which imply a decreased carbon fixation capacity and are in agreement with the well-known Fe deficiency induced impairment of the photosynthetic processes [26]. All proteins identified in the stress and defense category increased in abundance, and were related either to general defense [polyketide cyclase/dehydratase (spot *9*) and PR-5b (spot *12*)] or to defense against oxidative stress [thioredoxin reductase (spot *10*), glutathione peroxidase 1 (spot *11*) and glutaredoxin C4 (spot *13*)]. The polyketide cyclase/dehydratase contains a Betv1 domain and belongs to family 10 of plant pathogenesis-related proteins (PR-10; UniProt annotation) and PR-5b belongs to the thaumatin superfamily [48], both with yet unknown functions. However, some members of PR5 subfamily have been described to play distinctive roles in the defense system that protects against high-salt stress or osmotic imbalance [49], which is also likely to occur in the Fe-deficiency treatment in the presence of $CaCO_3$. The same PR5b protein showed increases in abundance in roots of *M. truncatula* plants grown in the presence of $CaCO_3$ [42]. Interestingly, a proteomic study on *Beta vulgaris* roots submitted to several levels of Zn toxicity, which also causes induced Fe-deficiency, found that some Bet v1 proteins, including some PR-10, increased in abundance in

Table 2
Relative molar abundance of G- and *S*-lignin derived markers, S/G ratio, percentage of protein markers and lignin/protein ratio in stems and petioles of Fe-sufficient and Fe deficient plants grown in the absence and presence of $CaCO_3$, as estimated by Py-GC/MS. Data are means ± SD of four biological replicates. Different letters within the same row and tissue indicate statistically significant differences using the Student's *t*-test and $p < 0.05$.

Compounds	Petioles			Stems		
	+Fe	−Fe	−Fe ± $CaCO_3$	+Fe	−Fe	−Fe ± $CaCO_3$
G-lignin markers						
Guaiacol	19.5 ± 0.5 a	24.7 ± 2.1 b	23.9 ± 2.2 b	25.6 ± 1.5 a	27.5 ± 2.1 a	26.2 ± 1.8 a
4-Methylguaiacol	3.4 ± 0.2 b	3.1 ± 0.2 a	3.0 ± 0.1 a	3.3 ± 0.4 a	3.4 ± 0.1 a	3.2 ± 0.1 a
4-Ethylguaiacol	4.0 ± 0.7 a	6.4 ± 0.2 b	6.5 ± 0.9 b	6.4 ± 0.4 a	7.1 ± 0.3 b	7.0 ± 0.7 ab
4-Vinylguaiacol	44.2 ± 2.4 c	36.2 ± 2.0 a	40.7 ± 2.4 b	23.5 ± 1.4 a	24.2 ± 1.2 a	25.2 ± 1.9 a
Eugenol	1.9 ± 0.2 b	1.4 ± 0.2 a	1.1 ± 0.3 a	1.0 ± 0.1 a	1.1 ± 0.1 a	1.1 ± 0.2 a
cis-Isoeugenol	1.5 ± 0.0 b	1.2 ± 0.2 a	1.0 ± 0.2 a	1.2 ± 0.1 a	1.2 ± 0.1 a	1.3 ± 0.1 a
trans-Isoeugenol	7.1 ± 0.2 a	7.0 ± 0.3 a	6.1 ± 0.9 a	6.4 ± 0.5 a	6.7 ± 0.7 a	7.1 ± 0.6 a
Total G compounds	81.6 ± 1.3 ab	80.1 ± 1.2 a	82.3 ± 1.3 b	67.5 ± 3.6 a	71.0 ± 1.6 a	71.1 ± 1.0 a
S-lignin markers						
Syringol	7.8 ± 0.6 a	9.1 ± 0.5 b	7.8 ± 0.9 a	15.2 ± 1.7 b	13.9 ± 0.5 b	12.8 ± 0.5 a
4-Methylsyringol	1.3 ± 0.1 b	1.2 ± 0.1 ab	1.0 ± 0.2 a	2.1 ± 0.1 b	1.7 ± 0.1 a	1.6 ± 0.1 a
4-Ethylsyringol	1.1 ± 0.2 a	1.6 ± 0.1 b	1.7 ± 0.3 b	3.2 ± 0.5 a	2.7 ± 0.2 a	2.9 ± 0.2 a
4-Vinylsyringol	5.7 ± 0.3 b	5.4 ± 0.4 ab	4.7 ± 0.6 a	8.0 ± 0.9 b	6.7 ± 0.5 a	6.7 ± 0.4 a
4-Allylsyringol	0.5 ± 0.1 a	0.4 ± 0.0 a	0.4 ± 0.1 a	0.5 ± 0.1 a	0.5 ± 0.1 ab	0.6 ± 0.0 b
cis-4-Propenylsyringol	0.3 ± 0.1 a	0.3 ± 0.1 a	0.3 ± 0.0 a	0.6 ± 0.1 a	0.5 ± 0.1 a	0.7 ± 0.1 a
trans-4-Propenylsyringol	1.7 ± 0.3 a	1.1 ± 0.1 a	1.8 ± 0.2 a	3.0 ± 0.4 a	3.0 ± 0.5 ab	3.7 ± 0.2 b
Total S compounds	18.4 ± 1.3 ab	19.9 ± 1.2 b	17.7 ± 1.3 a	32.5 ± 3.6 a	29.0 ± 1.6 a	28.9 ± 1.0 a
S/G ratio	0.2 ± 0.0 ab	0.3 ± 0.0 b	0.2 ± 0.0 a	0.5 ± 0.1 a	0.4 ± 0.0 a	0.4 ± 0.0 a
Protein markers*						
Phenylacetonitrile	42.9 ± 6.3 c	28.5 ± 5.5 b	12.9 ± 5.0 a	8.7 ± 1.8 b	9.3 ± 3.0 b	5.2 ± 1.4 a
Indole	138.0 ± 20.5 b	120.5 ± 16.0 b	76.7 ± 17.8 a	45.0 ± 5.2 a	57.2 ± 18.0 a	46.8 ± 15.8 a
3-Methylindole	35.9 ± 7.9 b	18.9 ± 4.1 a	15.1 ± 2.5 a	8.6 ± 1.3 a	10.0 ± 3.4 a	10.9 ± 2.8 a
Total protein markers*	216.8 ± 32.5 c	167.9 ± 25.1 b	104.7 ± 24.8 a	62.4 ± 8.2 a	76.5 ± 24.1 a	62.9 ± 19.9 a
Lignin/Protein ratio	0.5 ± 0.1 a	0.6 ± 0.1 b	1.0 ± 0.2 c	1.6 ± 0.2 a	1.4 ± 0.3 a	1.7 ± 0.4 a

* Protein-markers calculated as percentage of total lignin markers (G + S)

roots when Zn supply increased [39]. Therefore, we could speculate that the increases measured in both pathogenesis related proteins in the $CaCO_3$ treatment might be related to osmotic stress caused by both metal imbalances and the presence of $CaCO_3$. On the other hand, increases in proteins related to defense against oxidative stress including thioredoxin reductase (spot *10*) and those associated with glutathione metabolism, such as the glutathione peroxidase (spot *11*) and the glutaredoxin *C*4 (spot *13*), found in this study, have been reported to increase upon Fe deficiency in different root proteome studies [12] and are probably associated with the redox imbalances caused by the lack of Fe. The existence of osmotic and redox unbalances in the high pH treatment is also supported by the *de novo* detection of a pyridoxal biosynthesis protein (spot *31*). Pyridoxal, or vitamin B6, is a singlet oxygen quencher and may play a role in osmotic or salt tolerance as well as in oxidative stress resistance [50,51].

Changes in the protein-related category also indicate a Fe deficiency driven stress situation which was more severe in the presence of $CaCO_3$. Relative increases were observed in three proteins of the heat shock 70 kDa (HSP70) family whose members have direct functions in managing stress situations by preventing misfolded or damaged proteins to aggregate or by facilitating their disposal by interacting with ubiquitin ligases [52]. One of the HSP70 (spot *15*) increased in both Fe-deficiency treatments (although below the threshold level in the absence of $CaCO_3$), and its *Arabidopsis* counterpart (AtBIP1; At5g28540) is involved in the ER degradation of misfolded proteins (TAIR annotation). The decrease measured in the ubiquitin-conjugating enzyme (spot *14*) which belongs to the E2 class performing the second step in the ubiquitination pathway (UniProt annotation) may also suggest a role of the ubiquitin-dependent catabolic pathway in the Fe deficiency response. The other two HSP70 (spots *16* and *17*) increased only in the presence of $CaCO_3$ and are most likely isoforms of the same protein given their localization in the 2-DE gel (Supplementary Fig. S6B). These proteins blast to the same *Arabidopsis* orthologue (AtHsp70–10, At5g09590) that has been suggested to play an important role in the regulation of the Fe-S assembly pathway in mitochondria [53]. Their increases may be related to the decreases measured in Fe-S cluster proteins, including the NADH-ubiquinone reductase (spot *24*) of the respiratory chain complex I, the Fe-S subunit of the cytochrome b6f complex (spot *5*) and the ferredoxin nitrite reductase (spot *23*). On the other hand, significant changes in the protein translation machinery were only observed in the Fe deficiency treatment in the presence of $CaCO_3$, affecting two structural components of the ribosome (spots *19* and *21*) and an elongation factor (spot *20*). Changes in the abundance of some components of the ribosome induced by Fe deficiency have been described in *Arabidopsis* roots and authors speculated that these changes can control mRNA preference and bias translation efficiency towards specific sets of genes [11,54,55], but they also may indicate the need of *de novo* synthesis of Fe-deficiency effector proteins. The fact that these changes are only observed in the presence of $CaCO_3$ reinforces the strong effect of this treatment in the stem proteome.

Several lines of evidence support that Fe deficiency causes alterations in the cell wall of stem tissues, especially in the presence of $CaCO_3$. First, the increases in relative abundance measured in two protein species involved in the phenylpropanoid biosynthesis pathway: the phenylcoumaran benzylic ether reductase (PCBER, spot *29*) and a putative *O*-methyltrasferase similar to the caffeoyl-CoA *O*-methyltransferase 1 (spot *30*). PCBER has been shown to be one of the most abundant proteins in the xylem of poplar [56] that participates in lignan synthesis [57] and the *O*-methyltrasferase probably plays a role in the methylation steps necessary for the biosynthesis of monolignols, the lignin precursors [58]. Their increases suggest that Fe deficiency may cause changes in lignification. A second line of evidence is provided by the lignin Py-GC/MS analysis of the petioles, which showed a small but significant relative increase in the lignin per protein ratio in Fe-deficient petioles when compared to the controls, which was more intense in the presence than in the absence of $CaCO_3$ (Table 2). Finally, the microscopy study of petiole sections also indicates stronger alterations in plants grown in the presence than in the absence of $CaCO_3$. In petioles from plants grown in the presence of $CaCO_3$, phloroglucinol staining indicates an increase in lignin in the inner part of the xylem vessels (Fig. 4F), and the shift towards a green color in the autofluorescence signal in the same area suggests the existence of changes in lignin composition

(Fig. 4C); similar shifts in autofluorescence have been associated elsewhere with changes in lignin composition [59]. When Fe-deficient plants were grown in the absence of $CaCO_3$, changes in the micrograph images relative to the controls were less marked (Fig. 4B, E). Conversely to what occurs in the petioles, in the case of the stems from Fe-deficient plants the lignin/protein ratio, the lignin composition and the autofluorescence and phloroglucinol micrographs did not differ from those of control plants, and this is likely due to the fact that these stems were developed before the onset of Fe deficiency.

Overall, cell wall-related changes observed in petioles of plants grown in the presence of $CaCO_3$ should led to an increase in cell wall rigidity, especially in the xylem vessels. Changes in cell wall composition resulting in increased lignification have been described to occur upon mineral imbalances, for instance in the roots of Fe-deficient pear and quince cultivars [60], and have also been suggested as a detoxification strategy for excess Cd in roots [61,62]. Modification in cell wall related proteins have also been described in proteomic studies of Fe-deficient roots [12]. It has been hypothesized that increased lignification may provide a protective barrier to avoid the lateral transport and distribution of minerals by decreasing the permeability of the cell wall [63]. In leaves, Fe deficiency also elicits structural changes in morphology, including a reduction of the leaf xylem vessel size, which could disturb normal stomatal functioning [64,65].

Other effects of Fe deficiency in the stem protein profiles included increases in several spots identified as malate dehydrogenase (spots *25–27* in Table 1 and Supplementary Fig. S6C) and in a serine-hydroxymethyl-transferase (spot *28*) in both treatments that were also described in the proteome of Fe-deficient *M. truncatula* roots [42]. Increases in both proteins have been reported in physiological and proteomic studies on Fe deficiency in roots and leaves [12,66] and results from this study indicate this may be a common response throughout plant organs.

Mineral analyses indicate the existence of alterations in micro- and macronutrient balances as a result of Fe deficiency. Although the stem Fe concentrations did not decrease significantly in Fe-deficient plants grown in the absence of $CaCO_3$, Fe content decreases occurred in both Fe deficiency treatments (Fig. 3, Supplementary Fig. S3). The decrease in stem Fe concentration in the presence of $CaCO_3$ was accompanied at the proteomic level by decreases in relative abundance of three Fe containing proteins related to energy production: a subunit of a NADH-ubiquinone oxidoreductase (spot *24*), the ferredoxin-nitrite reductase (spot *23*), and the cytochrome b6-f complex (spot *5*). Decreases in abundance in Fe-containing, energy related proteins have been widely described in different proteomic studies as a result of Fe shortage [12], and this could ultimately account for the reduction in stem mass.

5. Conclusions

A summary of the proteomic results is shown in Fig. 5. Overall results indicate that Fe deficiency by itself has a mild effect on the stem proteome of *M. truncatula* plants, mainly affecting photosynthesis-related proteins. However, Fe deficiency in the presence of $CaCO_3$ has a stronger impact on the proteome, including a general increase in stress and protein metabolism related proteins not observed in Fe-deficient plants grown without $CaCO_3$, as well as a larger number of photosynthesis-related proteins decreasing. These results probably indicate the existence of mineral and osmotic unbalances. Iron deficiency also elicited significant increases in cell wall related proteins and in the lignin per protein ratio, which were more intense in the presence of $CaCO_3$. Changes in the lignin S and G monomer composition induced by Fe-deficiency and the microscopy study of petiole sections further confirm the existence of alterations in cell walls of petiole tissues. These results suggest that Fe-deficient plants, especially those grown in the presence of $CaCO_3$ as occurs in many arable soils, present an increased lignification and a probable lower capacity of cell walls to interact with ions in the xylem fluid, which ultimately may affect solute transport and distribution to the leaves.

Conflict of interest

Authors declare no conflict of interest.

Acknowledgements

Work supported by the Spanish Ministry of Science and Competitiveness (MINECO; projects AGL2012-31988, AGL2011-25379 and AGL2013-42175-R, co-financed by FEDER), the Aragón Government (group A03), and the US Department of Agriculture, Agricultural Research Service (under Agreement number 58-6250-0-008 to MAG). Support was obtained by contracts I3P-CSIC (JRC), FPI-MINECO (GL and LC-L), JAE-PRE-CSIC (EG-C) and JAE-DOC-CSIC (JR), co-financed by the European Social Fund. Authors thank A. Calviño for assistance in growing and harvesting plants. The contents of this publication do not

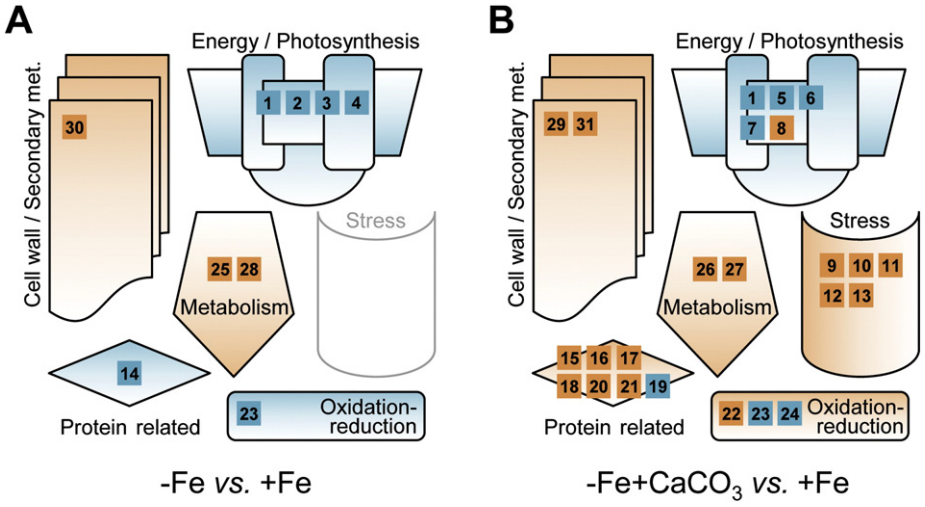

Fig. 5. Changes in metabolic pathways as affected by Fe deficiency without (A) and with $CaCO_3$ (B) when compared to Fe-sufficient plants. Pathways related to the identified proteins were integrated according to the GO annotation. A statistical Student *t*-test was performed to show relevant changes between samples. Orange symbols mark newly detected and proteins with increased relative abundance compared to controls (using a two-fold threshold change). The same threshold (decreases larger than 50%) was selected for proteins with decreased relative abundance (blue symbols). Numbers correspond to those in Table 1.

necessarily reflect the views or policies of the US Department of Agriculture, nor does mention of trade names, commercial products, or organizations imply endorsement by the US Government.

Appendix A. Supplementary data

Supplementary data to this article can be found online at http://dx.doi.org/10.1016/j.jprot.2016.03.017.

References

[1] J. Abadía, S. Vázquez, R. Rellán-Álvarez, H. El-Jendoubi, A. Abadía, A. Álvarez-Fernández, A.F. López-Millán, Towards a knowledge-based correction of iron chlorosis, Plant Physiol. Biochem. 49 (2011) 471–482.
[2] A. Álvarez-Fernández, P. Paniagua, J. Abadía, A. Abadía, Effects of Fe deficiency chlorosis on yield and fruit quality in peach (*Prunus persica* L. Batsch), J. Agric. Food Chem. 51 (2003) 5738–5744.
[3] K. Mengel, Iron availability in plant tissues – iron chlorosis on calcareous soils, Plant Soil 165 (1994) 275–283.
[4] B. Coulombe, R. Chaney, W. Wiebold, Bicarbonate directly induces iron chlorosis in susceptible soybean cultivars, Soil Sci. Soc. Am.J. 48 (1984) 1297–1301.
[5] D. Froelich, W. Fehr, Agronomic performance of soybeans with differing levels of iron deficiency chlorosis on calcareous soil, Crop Sci. 21 (1981) 438–441.
[6] S. Lin, S. Cianzio, R. Shoemaker, Mapping genetic loci for iron deficiency chlorosis in soybean, Mol. Breed. 3 (1997) 219–229.
[7] A. Álvarez-Fernández, J.C. Melgar, J. Abadía, A. Abadía, Effects of moderate and severe iron deficiency chlorosis on fruit yield, appearance and composition pear (*Pyrus communis* L.) and peach (*Prunus persica* L. Batsch), Environ. Exp. Bot. 71 (2011) 280–286.
[8] A. Rombolà, M. Tagliavini, Iron nutrition of fruit tree crops, in: L.L. Barton, J. Abadía (Eds.), Iron Nutrition in Plants and Rhizospheric Microorganisms, Springer, New York 2006, pp. 61–83.
[9] V. Romheld, Different strategies for iron acquisition in higher plants, Physiol. Plant. 70 (1987) 231–234.
[10] M.N. Hindt, M.L. Guerinot, Getting a sense for signals: regulation of the plant iron deficiency response, Biochim. Biophys. Acta 1823 (2012) 1521–1530.
[11] P. Lan, W. Li, T.N. Wen, J.Y. Shiau, Y.C. Wu, W. Lin, W. Schmidt, iTRAQ protein profile analysis of Arabidopsis roots reveals new aspects critical for iron homeostasis, Plant Physiol. 155 (2011) 821–834.
[12] A.F. López-Millán, M.A. Grusak, A. Abadía, J. Abadía, Iron deficiency in plants: an insight from proteomic approaches, Front. Plant Sci. 4 (2013) 254.
[13] R. Rellán-Álvarez, S. Andaluz, J. Rodríguez-Celma, G. Wohlgemuth, G. Zocchi, A. Álvarez-Fernández, O. Fiehn, A.F. López-Millán, J. Abadía, Changes in the proteomic and metabolic profiles of *Beta vulgaris* root tips in response to iron deficiency and resupply, BMC Plant Biol. 10 (2010) 120.
[14] R. Rellán-Álvarez, H. El-Jendoubi, G. Wohlgemuth, A. Abadía, O. Fiehn, J. Abadía, A. Álvarez-Fernández, Metabolite profile changes in xylem sap and leaf extracts of strategy I plants in response to iron deficiency and resupply, Front. Plant Sci. 2 (2011) 66.
[15] J. Rodríguez-Celma, W.D. Lin, G.M. Fu, J. Abadía, A.F. López-Millán, W. Schmidt, Mutually exclusive alterations in secondary metabolism are critical for the uptake of insoluble iron compounds by arabidopsis and *Medicago truncatula*, Plant Physiol. 162 (2013) 1473–1485.
[16] W. Schmidt, T.J. Buckhout, A hitchhiker's guide to the Arabidopsis ferrome, Plant Physiol. Biochem. 49 (2011) 462–470.
[17] D. Eide, M. Broderius, J. Fett, M.L. Guerinot, A novel iron-regulated metal transporter from plants identified by functional expression in yeast. Proc. Natl. Acad. Sci. U. S. A. 93 (1996) 5624–5628.
[18] N.J. Robinson, C.M. Procter, E.L. Connolly, M.L. Guerinot, A ferric-chelate reductase for iron uptake from soils, Nature 397 (1999) 694–697.
[19] S. Santi, W. Schmidt, Dissecting iron deficiency-induced proton extrusion in Arabidopsis roots, New Phytol. 183 (2009) 1072–1084.
[20] S. Cesco, G. Neumann, N. Tomasi, R. Pinton, L. Weisskopf, Release of plant-borne flavonoids into the rhizosphere and their role in plant nutrition, Plant Soil 329 (2010) 1–25.
[21] P. Fourcroy, P. Sisó-Terraza, D. Sudre, M. Saviron, G. Reyt, F. Gaymard, A. Abadía, J. Abadía, A. Álvarez-Fernández, J.F. Briat, Involvement of the ABCG37 transporter in secretion of scopoletin and derivatives by Arabidopsis roots in response to iron deficiency, New Phytol. 201 (2014) 155–167.
[22] J. Rodríguez-Celma, S. Vázquez-Reina, J. Orduna, A. Abadía, J. Abadía, A. Álvarez-Fernández, A.F. López-Millán, Characterization of flavins in roots of Fe-deficient strategy I plants, with a focus on *Medicago truncatula*, Plant Cell Physiol. 52 (2011) 2173–2189.
[23] N.B. Schmid, R.F. Giehl, S. Doll, H.P. Mock, N. Strehmel, D. Scheel, X. Kong, R.C. Hider, N. von Wiren, Feruloyl-CoA 6′-Hydroxylase1-dependent coumarins mediate iron acquisition from alkaline substrates in arabidopsis, Plant Physiol. 164 (2014) 160–172.
[24] A.F. López-Millán, F. Morales, Y. Gogorcena, A. Abadía, J. Abadía, Metabolic responses in iron deficient tomato plants, J. Plant Physiol. 166 (2009) 375–384.
[25] G. Zocchi, Metabolic changes in iron-stressed dicotyledoneus plants, in: L.L. Barton, J. Abadía (Eds.), Iron Nutrition in Plants and Rhizospheric Microorganisms, Springer, Dordrecht 2006, pp. 359–370.
[26] H. Marschner, Mineral Nutrition of Higher Plants, Academic Press, London, 1995.
[27] T.P. Durrett, W. Gassmann, E.E. Rogers, The FRD3-mediated efflux of citrate into the root vasculature is necessary for efficient iron translocation, Plant Physiol. 144 (2007) 197–205.
[28] R. Rellán-Álvarez, J. Giner-Martinez-Sierra, J. Orduna, I. Orera, J.A. Rodríguez-Castrillón, J.I. García-Alonso, J. Abadía, A. Álvarez-Fernández, Identification of a tri-iron(III), tri-citrate complex in the xylem sap of iron-deficient tomato resupplied with iron: new insights into plant iron long-distance transport, Plant Cell Physiol. 51 (2010) 91–102.
[29] H. Roschzttardtz, M. Seguela-Arnaud, J.F. Briat, G. Vert, C. Curie, The FRD3 citrate effluxer promotes iron nutrition between symplastically disconnected tissues throughout Arabidopsis development, Plant Cell 23 (2011) 2725–2737.
[30] M.W. Vasconcelos, M.A. Grusak, Morpho-physiological parameters affecting iron deficiency chlorosis in soybean (*Glycine* max L.), Plant and Soil 374 (2014) 161–172.
[31] W.J. Lucas, A. Groover, R. Lichtenberger, K. Furuta, S.R. Yadav, Y. Helariutta, X.Q. He, H. Fukuda, J. Kang, S.M. Brady, J.W. Patrick, J. Sperry, A. Yoshida, A.F. López-Millán, M.A. Grusak, P. Kachroo, The plant vascular system: evolution, development and functions, J. Integr. Plant Biol. 55 (2013) 294–388.
[32] Z. Hossain, S. Komatsu, Contribution of proteomic studies towards understanding plant heavy metal stress response, Front. Plant Sci. 3 (2013).
[33] J.V. Jorrín-Novo, A.M. Maldonado, S. Echevarria-Zomeno, L. Valledor, M.A. Castillejo, M. Curto, J. Valero, B. Sghaier, G. Donoso, I. Redondo, Plant proteomics update (2007–2008): second-generation proteomic techniques, an appropriate experimental design, and data analysis to fulfill MIAPE standards, increase plant proteome coverage and expand biological knowledge, J. Proteomics 72 (2009) 285–314.
[34] C. Liang, J. Tian, H. Liao, Proteomics dissection of plant responses to mineral nutrient deficiency, Proteomics 13 (2013) 624–636.
[35] V.A. Benedito, I. Torres-Jerez, J.D. Murray, A. Andriankaja, S. Allen, K. Kakar, M. Wandrey, J. Verdier, H. Zuber, T. Ott, S. Moreau, A. Niebel, T. Frickey, G. Weiller, J. He, X. Dai, P.X. Zhao, Y. Tang, M.K. Udvardi, A gene expression atlas of the model legume *Medicago truncatula*, Plant J. 55 (2008) 504–513.
[36] F. Colditz, H.P. Braun, *Medicago truncatula* proteomics, J. Proteomics 73 (2010) 1974–1985.
[37] B.S. Watson, V.S. Asirvatham, L. Wang, L.W. Sumner, Mapping the proteome of barrel medic (*Medicago truncatula*), Plant Physiol. 131 (2003) 1104–1123.
[38] N. Terry, Limiting factors in photosynthesis: I, Use of iron stress to control photochemical capacity in vivo. Plant Physiol. 65 (1980) 114–120.
[39] E. Gutierrez-Carbonell, G. Lattanzio, R. Sagardoy, J. Rodríguez-Celma, J.J. Rios Ruiz, A. Matros, A. Abadía, J. Abadía, A.F. López-Millán, Changes induced by zinc toxicity in the 2-DE protein profile of sugar beet roots, J. Proteome 94 (2013) 149–161.
[40] C.B. Garcia, M.A. Grusak, Mineral accumulation in vegetative and reproductive tissues during seed development in *Medicago truncatula*, Front. Plant Sci. 6 (2015) 622.
[41] J. Ralph, R.D. Hatfield, Pyrolysis-GC–MS characterization of forage materials, J. Agric. Food Chem. 39 (1991) 1426–1437.
[42] J. Rodríguez-Celma, G. Lattanzio, M.A. Grusak, A. Abadía, J. Abadía, A.F. López-Millán, Root responses of *Medicago truncatula* plants grown in two different iron deficiency conditions: changes in root protein profile and riboflavin biosynthesis, J. Proteome Res. 10 (2011) 2590–2601.
[43] M.R. Mártinez-Cuenca, F. Legaz, M.A. Forner-Giner, E. Primo-Millo, D.J. Iglesias, Bicarbonate blocks iron translocation from cotyledons inducing iron stress responses in Citrus roots, J. Plant Physiol. 170 (2013) 899–905.
[44] Y. Zuo, L. Ren, F. Zhang, R.F. Jiang, Bicarbonate concentration as affected by soil water content controls iron nutrition of peanut plants in a calcareous soil, Plant Physiol. Biochem. 45 (2007) 357–364.
[45] H.U. Kosegarten, B. Hoffmann, K. Mengel, Apoplastic pH and Fe^{3+} reduction in intact sunflower leaves, Plant Physiol. 121 (1999) 1069–1079.
[46] A.F. López-Millán, F. Morales, A. Abadía, J. Abadía, Effects of iron nutrition on the composition of the leaf apoplastic fluid and xylem sap in sugar beet: implication for iron and carbon transport, Plant Physiol. 124 (2000) 873–884.
[47] M. Nikolic, V. Römheld, Does high bicarbonate supply to roots change availability of iron in the leaf apoplast? Plant Soil 241 (2002) 67–74.
[48] B.L. Lytle, J. Song, N.B. de la Cruz, F.C. Peterson, K.A. Johnson, C.A. Bingman, G.N. Phillips Jr., B.F. Volkman, Structures of two *Arabidopsis thaliana* major latex proteins represent novel helix-grip folds, Proteins 76 (2009) 237–243.
[49] H. Tachi, K. Fukuda-Yamada, T. Kojima, M. Shiraiwa, H. Takahara, Molecular characterization of a novel soybean gene encoding a neutral PR-5 protein induced by high-salt stress, Plant Physiol. Biochem. 47 (2009) 73–79.
[50] H. Chen, L. Xiong, Pyridoxine is required for post-embryonic root development and tolerance to osmotic and oxidative stresses, Plant J. 44 (2005) 396–408.
[51] M. Tambasco-Studart, O. Titiz, T. Raschle, G. Forster, N. Amrhein, T.B. Fitzpatrick, Vitamin B6 biosynthesis in higher plants, Proc. Natl. Acad. Sci. U. S. A. 102 (2005) 13687–13692.
[52] J. Luders, J. Demand, J. Hohfeld, The ubiquitin-related BAG-1 provides a link between the molecular chaperones Hsc70/Hsp70 and the proteasome, J. Biol. Chem. 275 (2000) 4613–4617.
[53] L. Leaden, M.V. Busi, D.F. Gomez-Casati, The mitochondrial proteins AtHscB and Atlsu1 involved in Fe-S cluster assembly interact with the Hsp70-type chaperon AtHscA2 and modulate its catalytic activity, Mitochondrion 19 (Pt B) (2014) 375–381.
[54] P. Lan, W. Li, W. Schmidt, Complementary proteome and transcriptome profiling in phosphate-deficient Arabidopsis roots reveals multiple levels of gene regulation, Mol. Cell. Proteomics 11 (2012) 1156–1166.
[55] J. Rodríguez-Celma, I.C. Pan, W. Li, P. Lan, T.J. Buckhout, W. Schmidt, The transcriptional response of Arabidopsis leaves to Fe deficiency, Front. Plant Sci. 4 (2013) 276.
[56] D.R. Gang, H. Kasahara, Z.Q. Xia, K. Vander Mijnsbrugge, G. Bauw, W. Boerjan, M. Van Montagu, L.B. Davin, N.G. Lewis, Evolution of plant defense mechanisms,

Relationships of phenylcoumaran benzylic ether reductases to pinoresinol-lariciresinol and isoflavone reductases. J. Biol. Chem. 274 (1999) 7516–7527.
[57] K. Vander Mijnsbrugge, H. Beeckman, R. De Rycke, M. Van Montagu, G. Engler, W. Boerjan, Phenylcoumaran benzylic ether reductase, a prominent poplar xylem protein, is strongly associated with phenylpropanoid biosynthesis in lignifying cells, Planta 211 (2000) 502–509.
[58] C.T. Do, B. Pollet, J. Thevenin, R. Sibout, D. Denoue, Y. Barriere, C. Lapierre, L. Jouanin, Both caffeoyl Coenzyme A 3-O-methyltransferase 1 and caffeic acid O-methyltransferase 1 are involved in redundant functions for lignin, flavonoids and sinapoyl malate biosynthesis in Arabidopsis, Planta 226 (2007) 1117–1129.
[59] D. Djikanović, J. Simonović, A. Savić, I. Ristić, D. Bajuk-Bogdanović, A. Kalauzi, S. Cakić, J. Budinski-Simendić, M. Jeremić, K. Radotić, Structural Differences Between Lignin Model Polymers Synthesized from Various Monomers, J. Polym. Environ. 20 (2012) 607–617.
[60] S. Donnini, A. Castagna, A. Ranieri, G. Zocchi, Differential responses in pear and quince genotypes induced by Fe deficiency and bicarbonate, J. Plant Physiol. 166 (2009) 1181–1193.
[61] A. Lux, M. Vaculik, M. Martinka, D. Liskova, M.G. Kulkarni, W.A. Stirk, J. Van Staden, Cadmium induces hypodermal periderm formation in the roots of the monocotyledonous medicinal plant *Merwilla plumbea*, Ann. Bot. 107 (2011) 285–292.
[62] T. Redjala, I. Zelko, T. Sterckeman, V. Legué, A. Lux, Relationship between root structure and root cadmium uptake in maize, Environ. Exp. Bot. 71 (2011) 241–248.
[63] T. Higuchi, Biosynthesis of Lignin, In Plant Carbohydrates II, Springer, Berlin Heidelberg, 1981.
[64] T. Eichert, J.J. Peguero-Pina, E. Gil-Pelegrin, A. Heredia, V. Fernández, Effects of iron chlorosis and iron resupply on leaf xylem architecture, water relations, gas exchange and stomatal performance of field-grown peach (*Prunus persica*), Physiol. Plant. 138 (2010) 48–59.
[65] V. Fernández, T. Eichert, V. Del Río, G. López-Casado, J.A. Heredia-Guerrero, A. Abadía, J. Abadía, Leaf structural changes associated with iron deficiency chlorosis in field-grown pear and peach: physiological implications, Plant Soil 311 (2008) 161–172.
[66] J. Abadía, A.F. López-Millán, A. Rombolà, A. Abadía, Organic acids and Fe deficiency: a review, Plant Soil 241 (2002) 75–86.